



A modified model based state of charge estimation of power lithium-ion batteries using unscented Kalman filter

Yong Tian ^a, Bizhong Xia ^{a,*}, Wei Sun ^b, Zhihui Xu ^b, Weiwei Zheng ^b

^a Graduate School at Shenzhen, Tsinghua University, Shenzhen, Guangdong 518055, China

^b Sunwoda Electronic Co. Ltd., Shenzhen, Guangdong 518108, China



HIGHLIGHTS

- A modified equivalent circuit model is presented.
- A linear-averaging method is presented to compute correction factors.
- The UKF algorithm for SOC estimation based on the presented model is introduced.
- Performance of the proposed method is verified by comparison results.

ARTICLE INFO

Article history:

Received 22 January 2014

Received in revised form

17 July 2014

Accepted 23 July 2014

Available online 30 July 2014

Keywords:

Lithium-ion battery

State of charge

Modified equivalent circuit model

Unscented Kalman filter

ABSTRACT

Accurate estimation for the state of charge (SOC) is one of the most important aspects of a battery management system (BMS) in electric vehicles (EVs) as it provides drivers with the EVs' remaining range. However, it is difficult to get an accurate SOC, because its value cannot be directly measured and is affected by various factors, such as the operating temperature, current rate and cycle number. In this paper, a modified equivalent circuit model is presented to include the impact of different current rates and SOCs on the battery internal resistance, and the impact of different temperatures and current rates on the battery capacity. Besides, a linear-averaging method is presented to calculate the internal resistance and practical capacity correction factors according to data collected from the experimental bench and saved as look-up tables. The unscented Kalman filter (UKF) algorithm is then introduced to estimate the SOC according to the presented model. Experiments based on actual urban driving cycles are carried out to evaluate the performance of the presented method by comparing with two existed methods. Experimental results show that the proposed method can reduce the computation cost and improve the SOC estimation accuracy simultaneously.

© 2014 Elsevier B.V. All rights reserved.

1. Introduction

With the soaring energy crisis and environmental pollution, electric vehicles (EVs) have gained increased attention in recent years. Many industrialized nations have declared their plans for EVs development and production. For example, the US government has planned to have one million EVs on the road by 2015, and the Chinese government has set a goal of owning five million EVs by 2020 [1]. Power battery plays an important role in EVs, just like the oil does in the internal combustion engine vehicles (ICEVs). Comparing with other batteries, such as the lead-acid, nickel-cadmium and NiMH batteries, lithium-ion battery (LIB) has

merits in high voltage, high energy and power density, no memory effect, low self-discharge rate and long cycle life, so it has been widely used in EVs [2]. In the EVs application, accurate state of charge (SOC) estimation for LIB is essential to ease the "range anxiety" [1], realize the reasonable energy management and efficient utilization of the battery. Besides, it prevents the battery from over-charging or over-discharging that leads serious damage to the battery.

Previously, various methods for SOC estimation have been proposed. A common method is the Ampere-hour (Ah) counting method [3–5], in which the residual charge is calculated by integrating the current over time. The Ah method only needs to measure the battery current, so it is simple and can be easily implemented on-board. However, it requires accurate knowledge of the initial SOC value and suffers accumulated error from the integration process due to current drift. The open-circuit voltage

* Corresponding author. Tel.: +86 755 26036757.

E-mail address: xiabz@sz.tsinghua.edu.cn (B. Xia).

(OCV) [6,7] is another common method, which estimates the SOC based on the relationship between the OCV and the SOC. Nevertheless, it is not suitable for online estimation due to the long rest time to reach the battery's steady-state. Computational intelligence algorithms, such as the artificial neural networks (ANNs) [8–10], fuzzy-logic [11–13], and support vector machines (SVMs) [14–16] have also been developed to estimate the SOC. These methods do not require detailed knowledge of battery systems. Thus, they can be applied to all battery types and have excellent estimation performance if the training data are sufficient to cover the whole loading conditions. However, collecting training data that cover all of the loading conditions is time consuming and nearly impossible. Besides, all the aforementioned methods are open-loop estimation algorithms and do not require the battery model.

More recently, efforts have been focused on model-based and closed-loop estimation methods, among which the most famous two methods are the sliding mode observer (SMO) [17,18] and Kalman filter (KF) [1,19–26]. In these two methods, a battery is regarded as a power system and can be described by various models. They have high real-time and precise performance which strongly depends on the model accuracy related to its complexity.

A number of battery models have been proposed, such as the first principle models, black box models and equivalent circuit models (ECMs) [27]. Among them, the ECMs are widely used due to their advantages in simulating the dynamic behaviors of LIB [28,29]. Furthermore, LIB parameters, such as the practical capacity, internal resistance are related to operating temperature, current rate and cycle number. Therefore, corrections on battery parameters have been reported to improve the SOC estimation accuracy. In Ref. [1], the internal resistance was estimated online to improve the model accuracy. However, it increases the computation cost. In Ref. [29] and Ref. [30], variations of model parameters (e.g., the ohmic resistance, electrochemical polarization resistance and capacitance, concentration polarization resistance and capacitance) with the SOC have been discussed. However, the variations of battery capacity with temperature, current rate and cycle number are neglected. In Ref. [31], a cycle life model was developed to predict the battery capacity degradation with the increase of cycle, but the variations of battery capacity with the temperature and current rate, and the variations of internal resistance with the temperature, current rate and SOC are ignored. In Ref. [32], an enhanced battery model was presented to include the impact of different discharge rates and temperatures on the battery capacity. Unfortunately, it compensates the impact of different factors on battery capacity separately. Besides, the ohmic resistance is regarded as a state-variable in this method, leading to the increase of computation cost.

In this paper, a modified equivalent circuit model is presented. An offset voltage is employed to compensate the model error based on the fact that a small bias exists between the estimated OCV and the measured OCV [1]. To further improve the model accuracy, a combined resistance correction factor that simultaneously describes the variations of battery internal resistance with the current rate and SOC, as well as a combined capacity correction factor that simultaneously indicates the variations of battery capacity with the temperature and current rate are introduced. A linear-averaging method is proposed to calculate the values of the correction factors according to data collected from the experimental bench and saved as look-up tables. Comparing with the methods proposed in Ref. [1] and Ref. [32], the presented method compensates the impact of different temperatures and current rates on battery capacity simultaneously, so it is more accurate. Besides, the presented method compensates the impact of different current rates and SOCs on battery internal resistance with the look-up table method rather than the online estimation method, so it reduces the computation cost.

The following sections of this paper are organized as follows: Section 2 presents a modified simple equivalent circuit model and a linear-averaging method used to calculate the internal resistance and practical capacity correction factors. Section 3 introduces the UKF-based SOC estimation method with the presented battery model. Section 4 describes the experimental setup. Section 5 presents the experimental results and discussion, and Section 6 makes conclusions of the paper.

2. Battery modeling

2.1. Battery equivalent circuit model

The equivalent circuit models, consisting of resistors, capacitors and inductors, perform well in describing the battery dynamic characteristics, so they are usually used in SOC estimation [2,24,29]. A complicated model is able to accurately capture the characteristics of a battery, but it increases the computation cost which is not suitable for an on-board estimator [24]. On the contrary, a simple model can reduce the computation cost, but it may not be accurate enough to describe the LIB characteristics.

In this paper, a modified simple equivalent circuit model shown in Fig. 1 is presented to reduce the computation cost and improve the model accuracy. In this model, variable R represents the internal resistance at different current rates and SOCs, which can be calculated by a simple linear-averaging method (introduced in Section 2.3) according to the two-dimension R_b-I -SOC look-up table; OCV stands for the open circuit voltage (OCV), which is a nonlinear function of SOC; and V_c is introduced as an offset voltage based on the fact that a small bias exists between the estimated OCV and the measured OCV [1].

Based on Fig. 1, the discrete state-space equations can be derived as:

$$\text{SOC}(k+1) = \text{SOC}(k) - \frac{I(k) \times \Delta T}{Q_n} \quad (1)$$

$$V(k) = \text{OCV}[\text{SOC}(k)] - I(k) \times R(k) - V_c \quad (2)$$

where ΔT is the sample period, and Q_n represents the battery nominal capacity.

2.2. Model parameters estimation

In the presented equivalent circuit model shown Fig. 1, the parameters, including R , V_c and the OCV–SOC relationship need to be determined. In this paper, the battery's discharging internal resistance was tested as the following process:

- i) Charge the battery to its cut-off voltage with the standard charging method at the temperature of 25 °C;
- ii) Rest the battery for 1 h;

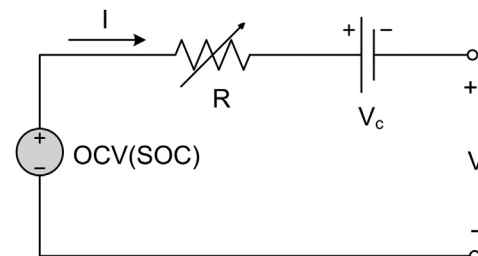


Fig. 1. Modified battery equivalent circuit model.

- iii) Measure the internal resistance;
- iv) Discharge the battery for 10% capacity with a constant current of I_x ;
- v) Rest the battery for 1 h;
- vi) Measure the internal resistance;
- vii) Return to step iv until the battery is fully discharged.

To study the impact of current rate and SOC on the internal resistance, the battery internal resistance was measured at different current rates and SOCs. The discharge current rate was set in the range of 0.1–2.0 with an interval of 0.2, and the SOC in the range of 0.1–1.0 with an interval of 0.1. The results are shown in Fig. 2, where KR represents the resistance correction factor and is defined as:

$$KR = \frac{R_x(I_x, SOC_x)}{R_r(1 C, 1)} \quad (3)$$

where $R_x(I_x, SOC_x)$ is the internal resistance with current I_x at SOC_x, and $R_r(1 C, 1)$ represents the internal resistance of the fully charged battery (SOC = 1) with the discharge current of 1 C, where C stands for the battery's nominal capacity.

In order to determine the relationship between the OCV and the SOC, an intermittent discharge test was carried out and a seventh-order polynomial fitting method was employed. The results are shown in Fig. 3, where the marks “o” represent the measured data, while the blue line (in web version) is the fitted curve. It can be seen that the seventh-order polynomial function is accurate enough to describe the OCV–SOC relationship.

2.3. Linear-averaging method

Internal resistance of a lithium-ion battery varies with the current rate, SOC, cycle number and operating temperature. In this paper, the former two factors are studied. In Section 2.2, the internal resistance has been measured at different current rates and different SOCs. To calculate the R_x and improve the model accuracy, this paper presents a linear-averaging method as shown in Fig. 4, where P_1 to P_4 are the four nearest points around point P_x in the look-up table. After I_x is measured and SOC_x is estimated, the corresponding R_x can be calculated by Eqs. (4)–(11):

$$KR_{14} = KR_1 + (KR_4 - KR_1) \frac{I_x - I_1}{I_2 - I_1} \quad (4)$$

$$KR_{23} = KR_2 + (KR_3 - KR_2) \frac{I_x - I_1}{I_2 - I_1} \quad (5)$$

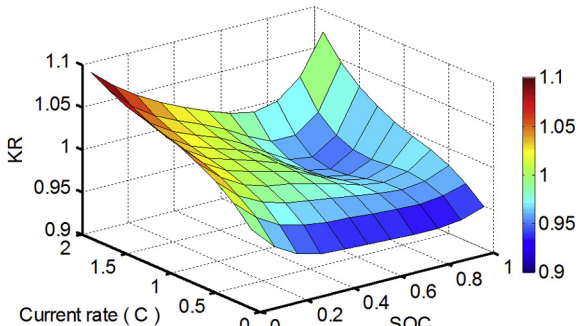


Fig. 2. Battery internal resistance vs. current rate and SOC.

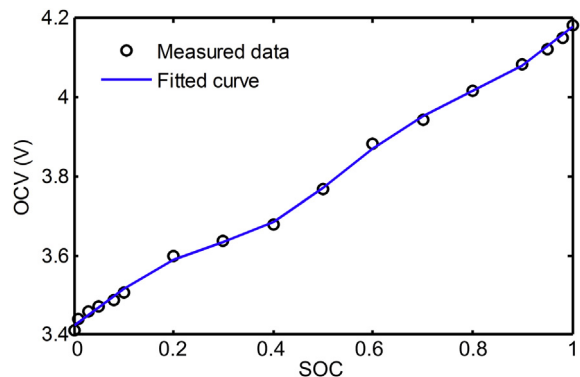


Fig. 3. Measured and fitted OCV vs. SOC.

$$KR_{x1} = KR_{14} + (KR_{23} - KR_{14}) \frac{SOC_x - SOC_1}{SOC_2 - SOC_1} \quad (6)$$

$$KR_{12} = KR_1 + (KR_2 - KR_1) \frac{SOC_x - SOC_1}{SOC_2 - SOC_1} \quad (7)$$

$$KR_{34} = KR_3 + (KR_4 - KR_3) \frac{SOC_x - SOC_2}{SOC_1 - SOC_2} \quad (8)$$

$$KR_{x2} = KR_{12} + (KR_{34} - KR_{12}) \frac{I_x - I_1}{I_2 - I_1} \quad (9)$$

$$KR_x = \frac{KR_{x1} + KR_{x2}}{2} \quad (10)$$

$$R_x = KR_x \times R_r \quad (11)$$

2.4. Battery practical capacity correction

It is well known that the practical capacity of a lithium-ion battery is affected by factors, such as the operating temperature, current rate and cycle number. In this paper, the former two factors are discussed. The calculated practical capacity at different temperatures and current rates are shown in Fig. 5, where the capacity correction factor KQ is defined as:

$$KQ = \frac{Q_p(T_x, I_x)}{Q_n(25^\circ\text{C}, 0.3 \text{ C})} \quad (12)$$

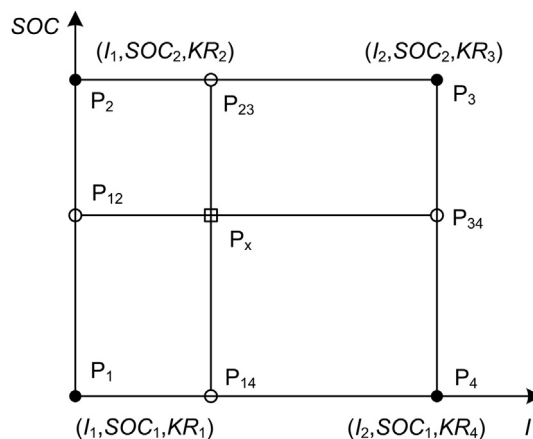


Fig. 4. Schematic diagram of the proposed linear-averaging method.

where $Q_p(T_x, I_x)$ is the practical capacity at the temperature of T_x and the current rate of I_x , and $Q_n(25^\circ\text{C}, 0.3 \text{ C})$ is the nominal capacity at the temperature of 25°C and the current rate of 0.3 C .

It should be noted that the maximum discharge current is lower than 2C according to the actual urban driving cycles test which will be introduced in Section 5, so in this paper the discharge current rate was limited within 2C . According to Fig. 5, it can be seen that the practical capacity slightly increases compared with the nominal capacity when the battery temperature is higher than the reference temperature of 25°C , but sharply reduces while the battery temperature is lower than 0°C . Besides, it slightly varies with the discharge current rate. The dynamic value of Q_p is also calculated by the proposed linear-averaging method described in Section 2.3.

3. UKF-based SOC estimation method

From the highly nonlinear profile of OCV vs. SOC shown in Fig. 3, it can be seen that the SOC estimation is a nonlinear problem. The extended Kalman filter (EKF) is a common approach for the nonlinear state estimation problem [33,34]. However, the EKF just uses the first-order or second-order terms of the Taylor series expansion to approximate a nonlinear model, which results in large error when the state-space model is highly nonlinear. Thus, the unscented Kalman filter (UKF) method that can address the approximation issues of the EKF is utilized in this paper. Instead of local linearization, the UKF captures the statistical distribution characteristics of a nonlinear system according to a series of sigma points [35–37]. The UKF-based estimation process can be summarized as follows:

i) Calculating weights associated with each sigma point:

$$\mathbf{W}_m^{[0]} = \frac{\lambda}{n + \lambda} \quad (13)$$

$$\mathbf{W}_c^{[0]} = \frac{\lambda}{n + \lambda} + (1 - \alpha^2 + \beta) \quad (14)$$

$$\mathbf{W}_m^{[i]} + \mathbf{W}_c^{[i]} = \frac{1}{2(n + \lambda)} \quad i = 1, 2, \dots, 2n \quad (15)$$

where \mathbf{W}_m and \mathbf{W}_c are sets of weighting matrices; n is the dimension of the state vector, in this paper, SOC is the unique state-variable, thus the value of n is one; α (in the range of $0\text{--}1$) and κ (default choice is $\kappa = 0$) are scaling parameters that determine the

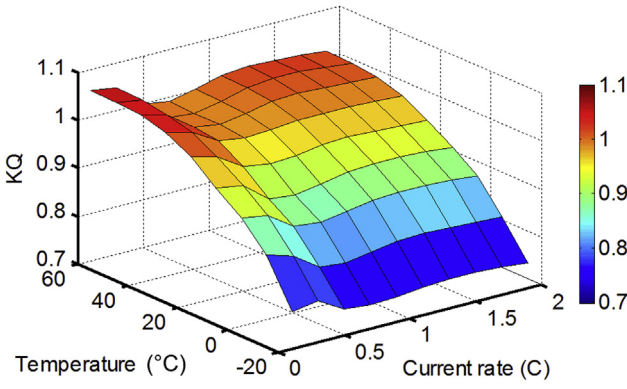


Fig. 5. Practical capacity vs. temperature and current rate.

spread of the sigma points around the mean value; β is used to incorporate the higher order knowledge about the distribution characteristics, for a Gaussian distribution, the optimal choice is $\beta = 2$.

ii) Calculating sigma points with mean SOC_{k-1}

$$\hat{\text{SOC}}_{k-1}^{[0]} = \text{SOC}_{k-1} \quad (16)$$

$$\hat{\text{SOC}}_{k-1}^{[i]} = \text{SOC}_{k-1} + \left(\sqrt{(n + \lambda)P_k} \right)_i \quad i = 1, 2, \dots, n \quad (17)$$

$$\hat{\text{SOC}}_{k-1}^{[n+i]} = \text{SOC}_{k-1} + \left(\sqrt{(n + \lambda)P_k} \right)_i \quad i = 1, 2, \dots, n \quad (18)$$

iii) Prediction update:

a. Propagating sigma points through the system/state equation:

$$\hat{\text{SOC}}_k = \hat{\text{SOC}}_{k-1} - \frac{I_{k-1}\Delta T}{KQ_{k-1}Q_n} \quad (19)$$

b. Calculating the mean of state variable:

$$\hat{\text{SOC}}_k = \sum_{i=0}^{2n} W_m^{[i]} \hat{\text{SOC}}_k^{[i]} \quad (20)$$

c. Calculating the propagated covariance:

$$\hat{P}_k = \sum_{i=0}^{2n} W_c^{[i]} (\hat{\text{SOC}}_k - \hat{\text{SOC}}_k^{[i]}) (\hat{\text{SOC}}_k - \hat{\text{SOC}}_k^{[i]})^T + Q_k \quad (21)$$

iv) Measurement update:

a. Propagating sigma points through the observation/measurement equation:

$$\hat{\mathbf{V}}_k = \text{OCV}_k - \mathbf{K}R_kR_lI_k - V_c \quad (22)$$

b. Calculating the mean of output variable:

$$\hat{V}_k = \sum_{i=0}^{2n} W_m^{[i]} \hat{\mathbf{V}}_k^{[i]} \quad (23)$$

c. Calculating the estimated covariance

$$\hat{P}_{yy} = \sum_{i=0}^{2n} W_c^{[i]} (\hat{V}_k - \hat{\mathbf{V}}_k^{[i]}) (\hat{V}_k - \hat{\mathbf{V}}_k^{[i]})^T + H_k \quad (24)$$

$$\hat{P}_{xy} = \sum_{i=0}^{2n} W_c^{[i]} (\hat{\text{SOC}}_k - \hat{\text{SOC}}_k^{[i]}) (\hat{V}_k - \hat{\mathbf{V}}_k^{[i]})^T \quad (25)$$

v) Measurement correction

a. Calculating the Kalman gain:

$$K_e = \hat{P}_{xy} \hat{P}_{yy}^{-1} \quad (26)$$

b. Updating the estimated state:

$$\text{SOC}_k = \hat{\text{SOC}}_k + K_e(V_k - \hat{V}_k) \quad (27)$$

c. Updating the propagated covariance:

$$P_k = \hat{P}_k - K_e \hat{P}_{yy} (K_e)^T \quad (28)$$

The flowchart of the UKF-based SOC estimation algorithm with the proposed model is shown in Fig. 6. At the beginning, the initial values of parameters, including α , β , κ , P_k , Q_k and H_k , are set. Afterward, the weights associated with each sigma point are calculated. In the main loop of the algorithm, the sigma points are calculated firstly. Battery current and voltage are measured per sample period. The capacity correction factor K_Q is calculated with the linear-average method described in Eqs. (4)–(11) before the prediction is updated, and the resistance correction factor K_R is calculated according to the same method before the measurement is updated. Finally, the measurement is corrected with the Kalman gain K_e .

4. Experimental configurations

As shown in Fig. 7, the test bench consists of a battery pack, a BMS module, a CAN communication unit, a convertor and a host computer. The battery pack, as shown in Fig. 8, is composed with 78 cells connected in series and 90 cells in parallel. The battery used in this test is Samsung ICR18650-22F-typed lithium-ion battery. Each cell has a nominal voltage of 3.62 V and a nominal capacity of 2.15 Ah. Therefore, the battery pack's nominal voltage and nominal capacity are 282 V and 193.5 Ah, respectively. The convertor is used to drive the motor or charge the battery according to the EV operating modes, including starting, running and braking. The host computer is used to calculate the model parameters and estimate the battery's SOC in real time. The BMS module samples the battery pack's voltage, current and temperature, transmits these sampling

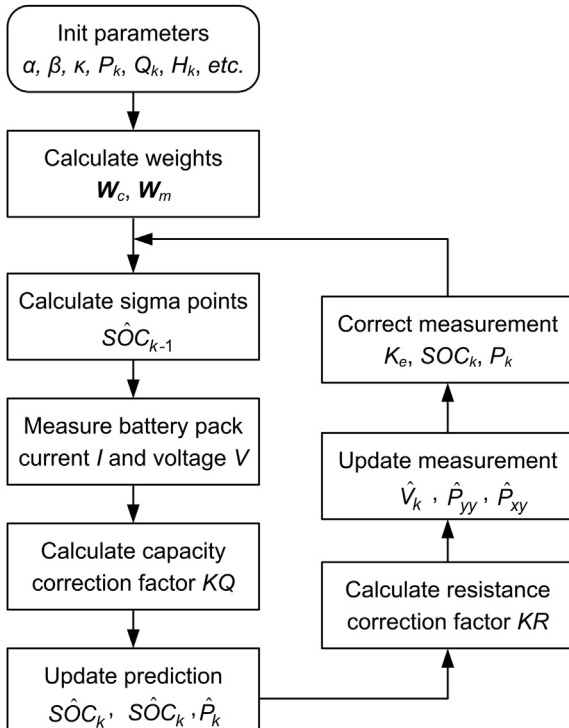


Fig. 6. Flowchart of the UKF-based estimator.

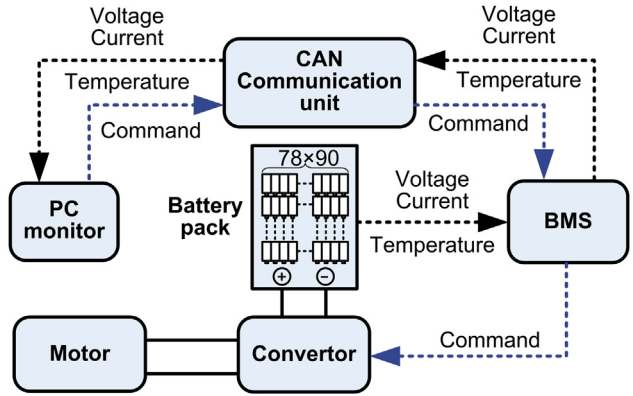


Fig. 7. Schematic diagram of the test bench.

data to the host computer and sends the control command to the convertor through the CAN communication unit.

An actual urban driving cycles test in Shenzhen (SZDC) is used to evaluate the performance of the proposed method. In the test, the pack's terminal voltage and current are measured per second. The current profile is shown in Fig. 9, in which negative current represents battery discharge while positive current means battery charge. From Fig. 9(b), it can be seen that the EV frequently starts, runs and brakes.

5. Results and discussion

5.1. Terminal voltage estimation

With the presented equivalent circuit model, the measured voltage and estimated voltage under SZDC test are shown in Fig. 10(a), and the corresponding voltage error is shown in Fig. 10(b). In Fig. 10(a), the blue dotted-line (in web version) is the reference voltage measured with a high precision sensor, while the red solid-line is the voltage estimated with the presented battery model. It can be seen that the presented model can well simulate the variation of the battery's terminal voltage, and the maximum error is less than 3%.

5.2. Practical capacity estimation

To evaluate the advantages of the proposed method in estimating the battery practical capacity. The estimated capacity using the proposed method is compared with that using the method proposed in Ref. [32]. With the Ref. [32] method, the battery capacity at different temperatures and current rates can be calculated by Eqs. (29)–(31).

$$KQ_T = -5.68 \times 10^{-5} T^2 + 5.59 \times 10^{-3} T + 0.921 \quad (29)$$

$$KQ_I = 1.88 \times 10^{-5} I^4 - 1.21 \times 10^{-3} I^3 + 1.34 \times 10^2 I^2 - 5.12 \times 10^2 I + 1.035 \quad (30)$$

$$Q_p = KQ_T \times KQ_I \times Q_n \quad (31)$$

The comparison results of capacity estimation are shown in Fig. 11 and Table 1. Fig. 11(a) shows the results at the temperature of 10 °C and different current rates of [0.1 1/3 1 2 3] C, and Fig. 11(b) shows the results at the current rate of 0.3 C and different temperatures of [-20 -10 0 25 45 60] °C. In Table 1, the Mean absolute

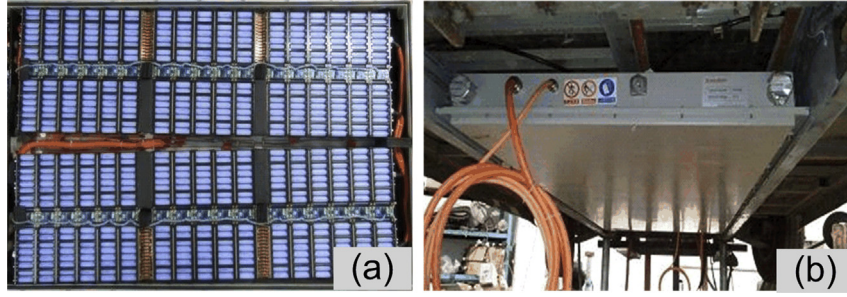


Fig. 8. Battery pack. (a) Internal view. (b) External view.

error (MAE) of the estimated voltage has the similar definition with that of the estimated SOC shown in Eq. (31) in Section 5.3. It is indicated that the proposed method has higher estimation accuracy than the Ref. [32] method, especially at different current rates when the temperature is much lower than 25 °C, for example 10 °C. The reason is that Ref. [32] method compensates the impact of different temperatures and current rates on battery capacity separately, while the proposed method compensates the impact simultaneously. Fig. 12 shows more details about the difference between the two methods. It can be seen that the Ref. [32] method compensates the impact of different temperatures with a constant current rate of 1/30 C, and compensates the impact of different current rates with a constant temperature of 25 °C. That's to say, with the Ref. [32] method, the practical capacity (Q_3) at temperature of T_x and current rate of CR_x is approximated by the production of Q_1 and Q_2 . Thus, under the condition that temperature is equal to 10 °C, the practical capacity estimated by the Ref. [32] method is

obviously higher than the actual values as shown in Fig. 11(a). The reason is that the battery capacity sharply reduces when the temperature is lower than 10 °C as shown in Fig. 2.

5.3. SOC estimation

Setting reference SOC to which the estimated values are compared is an important aspect for the SOC estimation experiments. In this paper, the reference SOC is obtained by the Ah method. To overcome the critical disadvantages of the Ah method: depending on initial SOC value and suffering accumulated error, two methods are employed as follows:

- 1) The battery pack is fully charged before it is discharged, thus its initial SOC can be accurately obtained as 100%.
- 2) A high accuracy current sensor is utilized to measure the battery pack current, so it is considered that the measured current is accurate enough to eliminate the accumulated error.

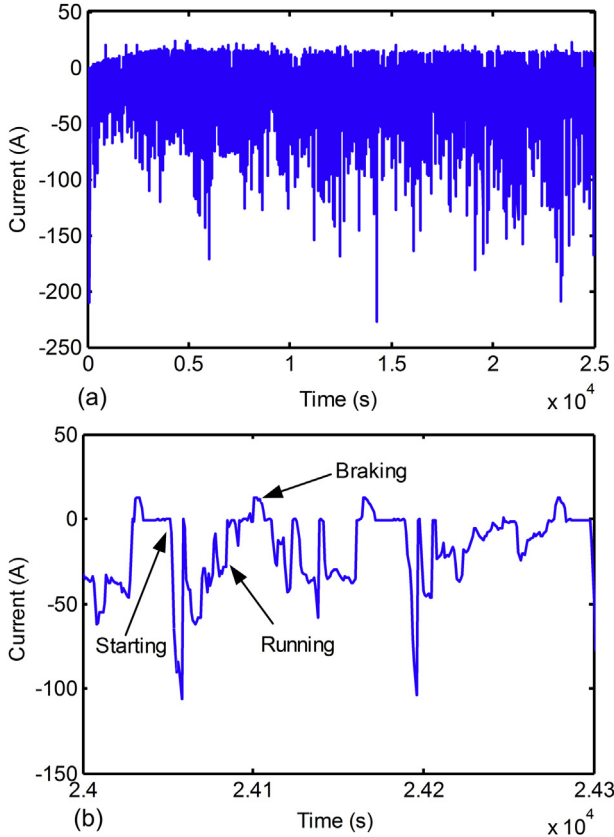


Fig. 9. Current profile under SZDC test. (a) Current vs. time profile. (b) Zoom figure for (a).

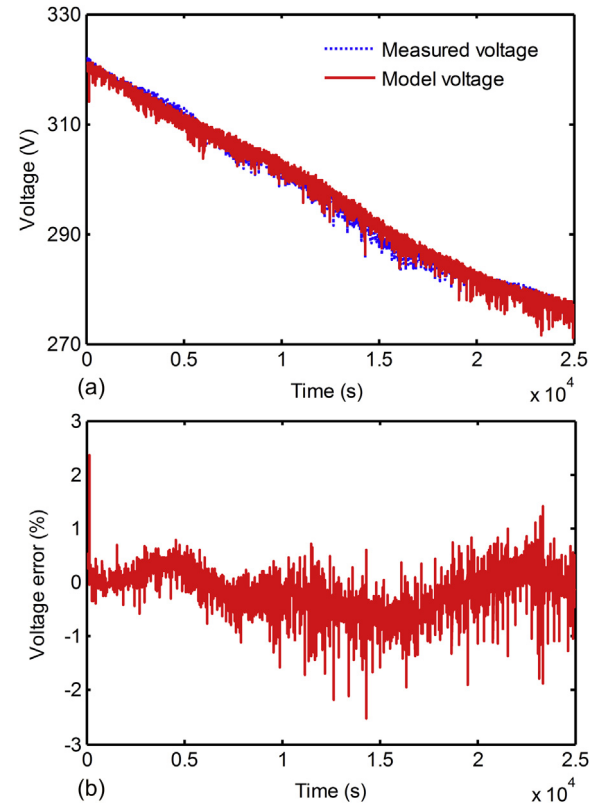


Fig. 10. Terminal voltage and voltage error under SZDC test. (a) Terminal voltage. (b) Voltage error.

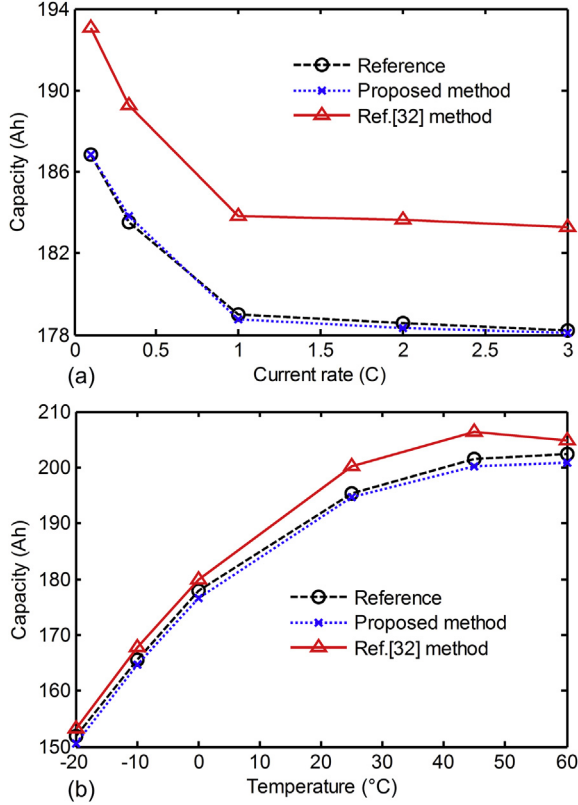


Fig. 11. Comparison of capacity estimation. (a) Capacity at the temperature of 10 °C and different current rates. (b) Capacity at the current rate of 0.3 C and different temperatures.

The parameters of the UKF algorithm are configured as follows:

$$Q_k = 0.0001, \quad H_k = 0.01, \quad \alpha = 1, \quad \beta = 2, \quad \kappa = 0.$$

Based on the presented equivalent circuit model shown in Fig. 1, as well as the linear-averaging method illustrated in Eqs. (4)–(11), the SOC estimation using UKF algorithm was implemented. The results are shown in Figs. 13(a) and 14(a), where the black dotted-line is the reference SOC, while the red solid-line (in web version) is the estimated values. From Fig. 14(a), it can be seen that the estimation error is always within 4%.

To further evaluate the performance of the proposed method, the SOC estimation results were compared with that estimated by the methods proposed in Ref. [1] and proposed in Ref. [32]. For all of the three methods, the same parameters of UKF algorithm were used. In this study, the SOC estimation accuracy and computation cost were compared. The computation cost was evaluated via the program execution time, which can be obtained by the MATLAB commands: tic and toc.

The mean absolute error (MAE) is used to evaluate the SOC estimation accuracy, and it is defined as [20]:

Table 1
Comparison of capacity error.

Methods	Results at different current rates		Results at different temperatures	
	Proposed method	Ref. [32] method	Proposed method	Ref. [32] method
Maximum error	0.34 Ah	6.21 Ah	1.58 Ah	4.89 Ah
MAE	0.18 Ah	5.39 Ah	1.24 Ah	2.84 Ah

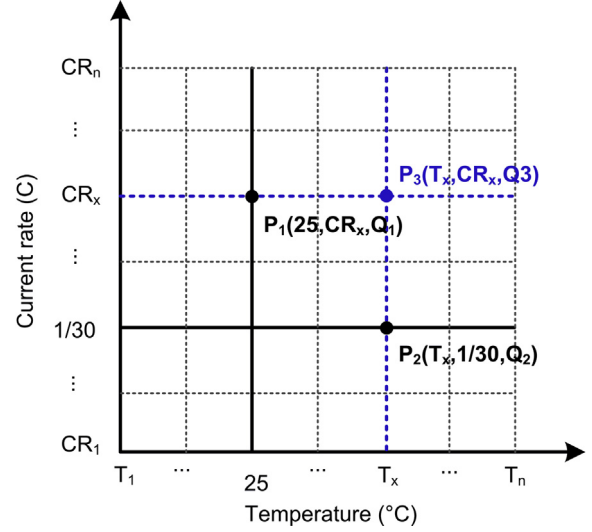


Fig. 12. Principle comparison of the proposed capacity correction method with the Ref. [32] method.

$$E_m = \frac{\sum_{i=1}^k |\text{SOC}_i - \hat{\text{SOC}}_i|}{k} \quad (32)$$

where E_m is the MAE, SOC_i and $\hat{\text{SOC}}_i$ are the actual and estimated SOC at time step i respectively.

The comparison results are shown in Figs. 13 and 14, as well as Table 2. Figs. 13(b) and 14(b) show the SOC values and the

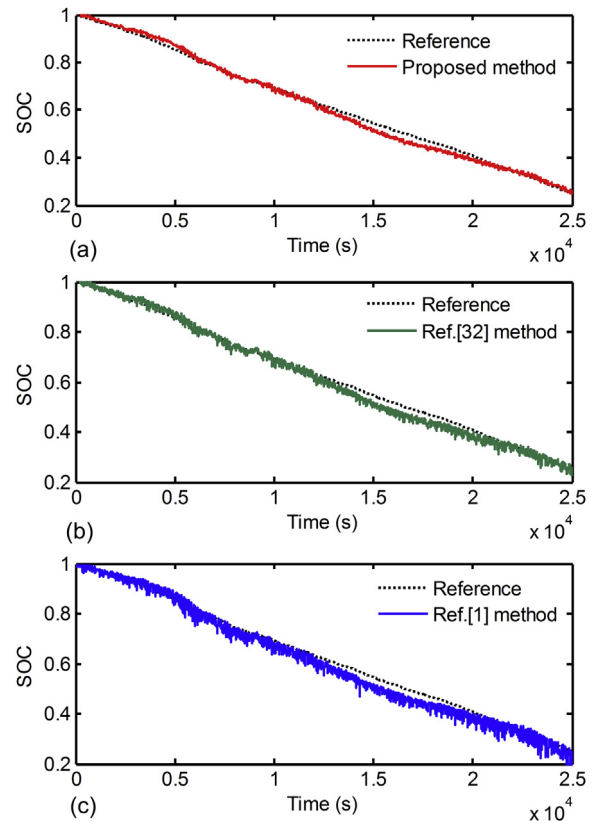


Fig. 13. Comparison of SOC estimation. (a) Proposed method. (b) Ref. [32] method. (c) Ref. [1] method.

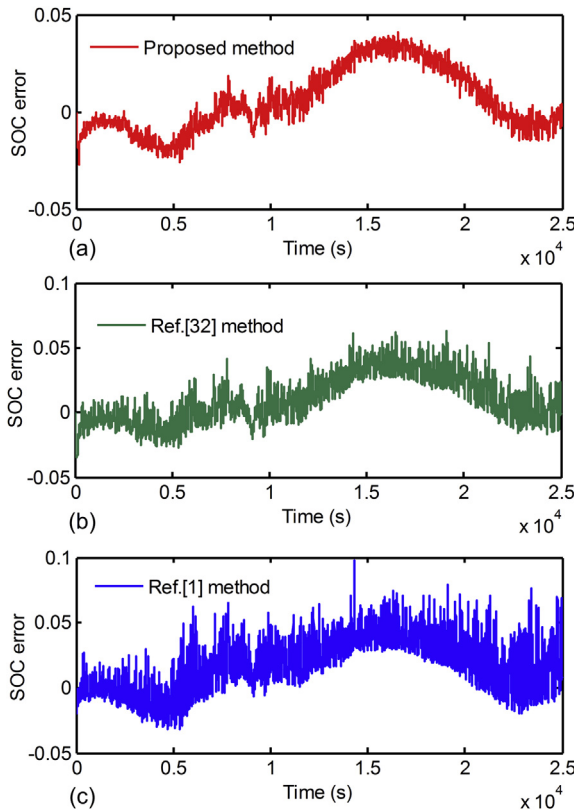


Fig. 14. Comparison of SOC error. (a) Proposed method. (b) Ref. [32] method. (c) Ref. [1] method.

corresponding errors estimated by the Ref. [32] method, while Figs. 13(c) and 14(c) show that estimated by the Ref. [1] method. Table 2 shows the comparison of the maximum SOC error, mean absolute error and computation cost. With all of the results, it is indicated that the proposed method can reduce the maximum SOC error by 44.2% compared with the Ref. [32] method, and the value is 57.6% compared with the Ref. [1] method. Besides, with the proposed method, the MAE can be respectively reduced by 41.6% and 42.9% compared with the Ref. [32] method and Ref. [1] method. Furthermore, the computation cost of the proposed method is 0.66 ms/point (millisecond per point), while the values of the Ref. [32] method and the Ref. [1] method are 1.14 ms/point and 0.96 ms/point respectively, which indicates that the proposed method can greatly reduce the computation cost. Therefore, comparing with the existed two methods, the proposed method is more suitable for online SOC estimation because it has lower requirements for the micro controller unit (MCU).

6. Conclusions

In this paper, a modified battery equivalent circuit model has been presented. A resistance correction factor is introduced to describe the impact of different current rates and SOCs on the battery internal resistance, and a capacity correction factor is used

to indicate the impact of different temperatures and current rates on the battery capacity. Besides, a linear-averaging method has been proposed to calculate the correction factors online. An estimator based on the unscented Kalman filter algorithm was designed to evaluate the proposed method according to data collected from the SZDC test. Experimental results show that the presented model well simulates the battery's terminal voltage variation with a maximum error of less than 3%, the capacity correction method has higher estimation accuracy than the Ref. [32] method, and the presented SOC estimation method can simultaneously reduce the computation cost and improve the SOC estimation accuracy compared with both the Ref. [1] method and the Ref. [32] method.

Acknowledgments

This work was supported by the China Postdoctoral Science Foundation Funded Project (2013M540941) and the Shenzhen Key Laboratory of LED Packaging Funded Project (NZDSY20120619141243215).

References

- [1] W. He, N. Williard, C.C. Chen, M. Pecht, *Microelectron. Reliab.* 53 (2013) 840–847.
- [2] J.H. Li, J.K. Barillas, C. Guenther, M.A. Danzer, *J. Power Sources* 230 (2013) 244–250.
- [3] J.H. Taylor, B.W. Johnson, *IEEE Trans. Ind. Electron.* 39 (1992) 398–409.
- [4] T.H. Liu, D.F. Chen, C.C. Fang, *Int. J. Electron.* 87 (2000) 211–226.
- [5] K.S. Ng, C.S. Moo, Y.P. Chen, Y.C. Hsieh, *Appl. Energy* 86 (2009) 1506–1511.
- [6] S. Lee, J. Kim, J. Lee, B.H. Cho, *J. Power Sources* 185 (2008) 1367–1373.
- [7] V. Pop, H.J. Bergveld, P.H.L. Notten, P.P.L. Regtien, *Meas. Sci. Technol.* 16 (2005) R93–R110.
- [8] G. Capizzi, F. Bonanno, C. Napoli, in: *3rd Int. Conf. Clean Electr. Power: Renew. Energy Resour. Impact*, Ischia, 2011, pp. 341–344.
- [9] H.X. Lu, Y. Lu, Z.F. Tang, S.J. Wang, in: *Int. Conf. Comput. Intell. Nat. Comput.*, Jinan, 2006, pp. 133–137.
- [10] M. Charkhgard, M. Farrokhi, *IEEE Trans. Ind. Electron.* 57 (2010) 4178–4187.
- [11] A.J. Salkind, C. Fenner, P. Singh, T. Atwater, D.E. Reisner, *J. Power Sources* 80 (1999) 293–300.
- [12] P. Singh, R.R. Vinjamuri, X.Q. Wang, D. Reisner, *J. Power Sources* 162 (2006) 829–836.
- [13] S. Malkhandi, *Eng. Appl. Artif. Intell.* 19 (2006) 479–485.
- [14] T. Hansen, C.J. Wang, *J. Power Sources* 141 (2005) 351–358.
- [15] Q. Shi, C. Zhang, N. Cui, *Int. J. Autom. Technol.* 9 (2008) 759–764.
- [16] X.S. Hu, F.C. Sun, in: *Int. Conf. Intelligent Hum.-Mach. Syst. Cybern.*, IHMSC, Hangzhou, 2009, pp. 392–396.
- [17] I.S. Kim, *J. Power Sources* 163 (2006) 584–590.
- [18] X.P. Chen, W.X. Shen, Z.W. Cao, A. Kapoor, I. Hijazin, in: *IEEE Conf. Ind. Electron. Appl. Proc.*, Melbourne, 2013, pp. 601–606.
- [19] J. Lee, O. Nam, B.H. Cho, *J. Power Sources* 174 (2007) 9–15.
- [20] J.Y. Wang, J.G. Guo, L. Ding, *Energy Convers. Manage.* 50 (2009) 3182–3186.
- [21] J.Y. Han, D.C. Kim, M. Sunwoo, *J. Power Sources* 188 (2009) 606–612.
- [22] F.C. Sun, X.S. Hu, Y. Zou, S.G. Li, *Energy* 36 (2011) 3531–3540.
- [23] H.F. Dai, X.Z. Wei, Z.C. Sun, J.Y. Wang, W.J. Gu, *Appl. Energy* 95 (2012) 227–237.
- [24] C. Hu, B.D. Youn, J. Chung, *Appl. Energy* 92 (2012) 694–704.
- [25] G.L. Plett, *J. Power Sources* 161 (2006) 1356–1384.
- [26] X.S. Hu, F.C. Sun, Y. Zou, *Simul. Model. Pract. Theory* 34 (2013) 1–11.
- [27] S. Cho, H. Jeong, C.H. Han, S.S. Jin, J.H. Lim, J. Oh, *Comput. Chem. Eng.* 41 (2012) 1–9.
- [28] R.C. Kroese, P.T. Krein, in: *IEEE Annu. Power Electron. Spec. Conf.*, Rhodes, 2008, pp. 1336–1342.
- [29] H.W. He, R. Xiong, X.W. Zhang, F.C. Sun, J.X. Fan, *IEEE Trans. Veh. Technol.* 60 (2011) 1461–1469.
- [30] X.P. Chen, W.X. Shen, Z.W. Cao, A. Kapoor, *J. Power Sources* 246 (2014) 667–678.
- [31] L.W. Kang, X. Zhao, J. Ma, *Appl. Energy* 121 (2014) 20–27.
- [32] Z.W. He, M.Y. Gao, C.S. Wang, L.Y. Wang, Y.Y. Liu, *Energies* 6 (2013) 4134–4151.
- [33] R.E. Kalman, *Trans. ASME J. Basic Eng.* 82 (1960) 35–45.
- [34] K. Xiong, H. Zhang, L. Liu, *IET Control Theory Appl.* 2 (2008) 239–250.
- [35] K. Nosrati, A.S. Rostami, A. Azemi, N. Pariz, in: *Int. Conf. Adv. Comput. Control.*, Harbin, 2011, pp. 378–383.
- [36] R. Van der Merwe, E. Wan, in: *IEEE Int. Conf. Acoust. Speech Signal Process Proc.*, Hong Kong, 2003, pp. 701–704.
- [37] A. Mirzaee, K. Salahshoor, *J. Process Control* 22 (2012) 626–634.

Table 2

Comparison of SOC error and computation cost.

Methods	Proposed method	Ref. [32] method	Ref. [1] method
Maximum error	4.12%	7.38%	9.72%
MAE	1.25%	2.14%	2.19%
Computation cost	0.66 ms/point	1.14 ms/point	0.97 ms/point